TRANSLATION

Mechanisms that ensure speed and fidelity in eukaryotic translation termination

Michael R. Lawson[1]†, Laura N. Lessen[2,3]†, Jinfan Wang[1], Arjun Prabhakar[1]‡, Nicholas C. Corsepius[1]§, Rachel Green[3,4]*, Joseph D. Puglisi[1]*

Translation termination, which liberates a nascent polypeptide from the ribosome specifically at stop codons, must occur accurately and rapidly. We established single-molecule fluorescence assays to track the dynamics of ribosomes and two requisite release factors (eRF1 and eRF3) throughout termination using an in vitro–reconstituted yeast translation system. We found that the two eukaryotic release factors bound together to recognize stop codons rapidly and elicit termination through a tightly regulated, multistep process that resembles transfer RNA selection during translation elongation. Because the release factors are conserved from yeast to humans, the molecular events that underlie yeast translation termination are likely broadly fundamental to eukaryotic protein synthesis.

Protein synthesis concludes when a translating ribosome encounters a stop codon at the end of an open reading frame, triggering recruitment of two factors to liberate the nascent polypeptide: eukaryotic release factor 1 (eRF1), a tRNA-shaped protein that decodes the stop codon in the ribosomal aminoacyl-tRNA site (A site) and cleaves the peptidyl-tRNA bond (*1*–*3*), and eukaryotic release factor 3 (eRF3), a GTPase that promotes eRF1 action (*4*–*6*). After translation termination, the ribosome, peptidyl-tRNA site (P site) tRNA, and mRNA are released by recycling (*4*, *7*, *8*). Despite decades of study, the order and timing of the molecular events that drive translation termination remain unclear because multistep processes are difficult to assess using traditional approaches. A cohesive understanding of translation termination and its underlying steps that are central to normal translation would also support the treatment of diseases caused by premature stop codons, which include cystic fibrosis, muscular dystrophy, and hereditary cancers (*9*). Because premature stop codons cause 11% of all heritable human diseases (*10*), stop codon readthrough therapeutics have immense clinical potential (*9*, *11*).

Direct tracking of release factor dynamics

Here, we used an in vitro–reconstituted yeast translation system (*12*) and single-molecule fluorescence spectroscopy to track eukaryotic release factor dynamics and termination directly. We reasoned that ribosomes translating mRNAs with very short open reading frames would provide the simplest system for detailed analysis of the discrete substeps of termination. Ribosome complexes were programmed with Met (M-Stop) or Met-Phe (M-F-Stop) mRNAs, achieved by incubation with purified Met-tRNA$^{Met}_i$, initiation factors, elongation factors, and tRNAs (as appropriate) and then reacted with saturating amounts of eRF1 and eRF3 (*13*). Peptide release from both M-Stop and M-F-Stop ribosome complexes occurred at similar rates as a longer tetrapeptide (M-F-K-K-Stop)–programmed ribosome complex (Fig. 1A and fig. S1, A and B) and also matched the rate previously characterized for tripeptide-programmed ribosome complexes (*4*, *5*). To monitor eRF1 and eRF3 binding to ribosomes in real time, we labeled both proteins specifically with fluorescent dyes (fig. S1, C and D) and established that the labeled proteins exhibited wild-type peptide release activity (Fig. 1B and fig. S1, E and F). Association of eRF1 with the ribosome was monitored by Förster resonance energy transfer (FRET) between 60*S* subunits labeled with Cy3 (FRET donor) on the C terminus of uL18 (*14*) and eRF1 labeled with Cy5 (FRET acceptor) on the N terminus. Structural models placed these termini ~50 Å apart when eRF1 was bound in the A site (Fig. 1C) (*3*, *15*). Next, Cy3-labeled ribosomal complexes programmed with Met in the P site and either UAA or UUC in the A site were combined with Cy5-eRF1 and unlabeled eRF3, and FRET was monitored at equilibrium using total internal reflection fluorescence microscopy. eRF1-60*S* FRET was only observed when a stop codon was in the A site (Fig. 1D and fig. S1, G and H), demonstrating the specificity of the FRET signal for proper eRF1 association mediated by a stop codon.

We leveraged this FRET-based binding signal to determine the roles of eRF1 and eRF3 in translation termination. We first prepared 80*S* ribosomal complexes programmed on 5′-biotinylated M-Stop mRNAs with Cy5-labeled 60*S* subunits; these complexes were tethered to neutravidin-coated zero-mode waveguide (ZMW) surfaces (*16*, *17*). Upon start of real-time data acquisition, Cy3-eRF1, excess GTP, and unlabeled eRF3 were added to ZMWs, and Cy3-eRF1 and Cy5-60*S* fluorescence within individual ZMWs was monitored by excitation with a 532-nm laser (Fig. 2A).

Rapid, concentration-dependent eRF1 binding to the ribosomal A site was detected upon delivery of the release factors (Fig. 2, B to D, and fig. S2, A to C). Association kinetics were fit to a double-exponential function with a dominant (56 to 83%) eRF1 concentration–dependent fast phase with a pseudo–second-order rate constant of 6.3 ± 3.9 $\mu M^{-1}\ s^{-1}$ [95% confidence interval (CI); Fig. 2, D and E, and fig. S2B]; a minor (17 to 44%) slow phase, which did not vary with eRF1 concentration, was also observed (e.g., k_{obs} = ~0.009 s^{-1}; Fig. 2E and fig. S2B). Conversely, eRF1 bound very slowly to these same complexes in the absence of eRF3 (e.g., k_{obs} = ~0.008 s^{-1}; Fig. 2, E and F, and fig. S2, D and E); the rate constant for this eRF3-independent binding was similar to the slow phase observed with eRF3 and also was unaffected by eRF1 concentration. In all cases, eRF1-binding events were long-lived (e.g., τ = 227 ± 13 s; fig. S2, B and E), and prolonged detection was likely limited by the dye photobleaching lifetime (fig. S2F). In the presence of eRF3, the rapid eRF1 binding observed here was similar to the rate of Phe-tRNA^{Phe} ternary complex binding to its cognate A-site codon under similar conditions (9.0 ± 0.4 $\mu M^{-1}\ s^{-1}$; fig. S2G). These results indicate that eRF1 binding, which would otherwise be limited by a slow event, is rapid enough to compete with tRNAs for A-site occupancy when assisted by eRF3.

We next tracked eRF3 dynamics directly, independently of eRF1, to establish a baseline understanding of its interaction with the ribosome. We used a previously established inter-ribosomal subunit FRET signal to confirm 80*S* complex formation (*14*) and monitored dye-labeled eRF3 dynamics by fluorescent bursts that occured upon factor binding to immobilized ribosomes. Ribosomes, Cy3 labeled on uL18, and Cy5 labeled on uS19 (yielding FRET upon 80*S* formation) were programmed with 5′-biotinylated M-Stop mRNAs and tethered to ZMWs. Next, Cy5-eRF3 and GTP were added to ZMWs and illuminated with 532- and 642-nm lasers. After an initial phase of FRET, typified by rapid Cy5-40*S* photobleaching, brief bursts of additional Cy5 signal were observed that marked binding and dissociation of eRF3 (Fig. 3, A and B). eRF3 binding was concentration dependent (Fig. 3C), and association kinetics were fit to an exponential function with a pseudo–second-order rate constant of

[1]Department of Structural Biology, Stanford University School of Medicine, Stanford, CA, USA. [2]Program in Molecular Biophysics, Johns Hopkins University School of Medicine, Baltimore, MD, USA. [3]Department of Molecular Biology and Genetics, Johns Hopkins University School of Medicine, Baltimore, MD, USA. [4]Howard Hughes Medical Institute, Johns Hopkins University School of Medicine, Baltimore, MD, USA
*Corresponding author. Email: ragreen@jhmi.edu (R.G.); puglisi@stanford.edu (J.D.P.)
†These authors contributed equally to this work.
‡Present address: Pacific Biosciences Inc., Menlo Park, CA, USA.
§Present address: Department of Chemistry, Fresno City College, Fresno, CA, USA.

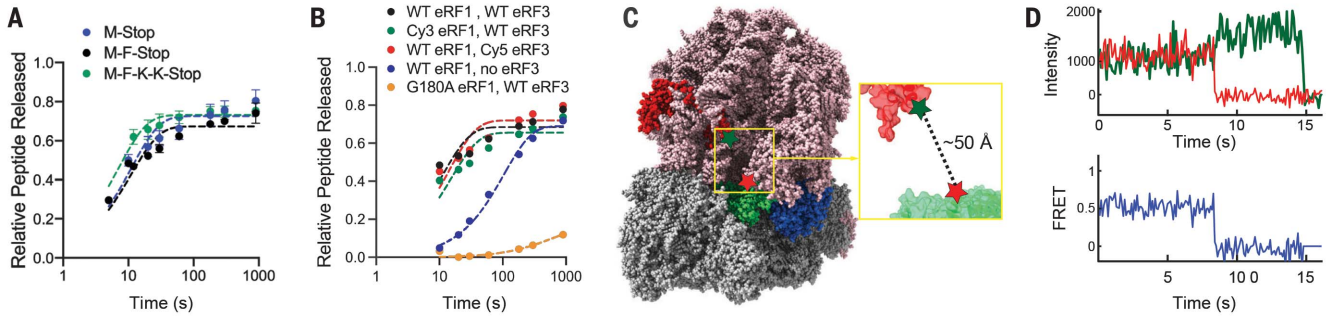

Fig. 1. Bulk biochemical and single-molecule studies of termination. (**A**) Peptides are liberated at similar rates from ribosomes translating a variety of model mRNAs. (**B**) Wild-type and labeled release factors liberate peptides from ribosomes. Catalytically dead eRF1 (orange) is inactive. (**C**) Structural modeling [Protein Data Bank (PDB) ID: 5LZT (*15*)] suggests that labeled eRF1 (green, Cy5 labeled at red star) would FRET with ribosomes (red, Cy3 labeled at green star) upon binding to the A site. (**D**) Example of FRET observed with Cy3-eRF1 and Cy5-60S by total internal reflection fluorescence microscopy.

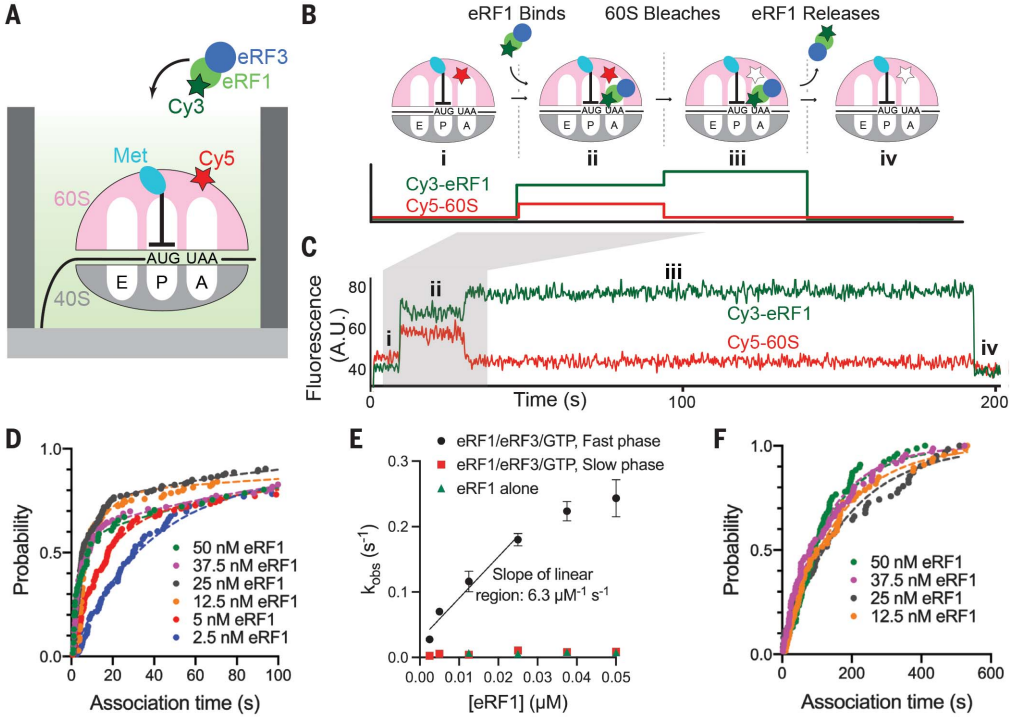

Fig. 2. eRF3 promotes fast binding of eRF1 to ribosomes halted at stop codons. (**A**) Experimental setup. (**B**) Assay schematic. (**C**) Example of fast binding of eRF1 (Cy3, green) to M-Stop ribosomes (Cy5, red) observed in the presence of eRF3. (**D**) Binding of eRF1 to M-Stop ribosomes is fast and concentration dependent in the presence of eRF3. Association time distributions were fit to a double-exponential model. (**E**) Observed rates of eRF1 binding to M-Stop ribosomes (k_{obs}) with and without eRF3. The plateau observed with the eRF1/eRF3/GTP fast phase coincides with the rate of sample mixing in ZMWs (*17*). (**F**) Binding of eRF1 to M-Stop ribosomes is slow and eRF1 concentration independent without eRF3. Association time distributions were fit to an exponential model.

$0.4 \pm 0.2\ \mu M^{-1}\ s^{-1}$ (95% CI; fig. S3, A and B). eRF3 resided briefly on the ribosome ($\tau = 0.15 \pm 0.01$ s; Fig. 3D), and the dwell times between eRF3-binding events varied with its concentration (fig. S3B), consistent with a bimolecular association reaction. Inclusion of GTP analogs, GDP, or a GTPase-deficient eRF3 mutant [H348E (*4*)] did not markedly affect the association or dissociation rates of eRF3 (about twofold or less; Fig. 3D and fig. S3C) suggesting that this binding cycle occurs independently of the eRF3 nucleotide–bound state or GTP hydrolysis.

Two distinct models could explain how eRF3 promotes the fast association of eRF1 with ribosomes halted at stop codons. eRF3 may first bind to ribosomes, triggering rearrangements that favor subsequent association of eRF1 with ribosomes. Alternatively, eRF3 may act as a chaperone, directly delivering eRF1 to ribosomes (*5*). To distinguish between these models, we performed single-molecule experiments similar to those described above but now simultaneously tracking fluorescent eRF1 and eRF3. We observed concurrent binding of the two factors to M-Stop ribosomes (Fig. 4, A and B). Although we also observed eRF1 and/or eRF3 binding individually to ribosomes in these experiments (which was unsurprising because the release factors can each bind alone to ribosomes and are at subsaturating concentrations), the likelihood of such independent binding events occurring simultaneously was very low (<0.1%), allowing us to rule out that co-arrivals happen primarily by random chance (see the materials and methods). Analysis of Cy5 (eRF1) and Cy3.5 (eRF3) fluorescence intensities, aligned to the beginning of apparent co-association events ("postsynchronization"), further demonstrated that eRF3 binding to a stop codon–halted ribosome is transient, whereas eRF1 resides longer on the ribosome (Fig. 4C). Omission of GTP decreased the number of observed co-binding events by 17-fold, confirming that eRF1, eRF3, and GTP bind the ribosome together as a preformed ternary complex (fig. S4A). Ternary complex association kinetics were fit to a double-exponential function, yielding a dominant fast-phase rate that was dependent upon eRF1 concentration and a pseudo–second-order rate constant of $2.6 \pm 5.1\ \mu M^{-1}\ s^{-1}$ (95% CI; Fig. 4D and fig. S4, B to D). In contrast to the dynamics of eRF3 in absence of eRF1 (where eRF3 lifetime had little

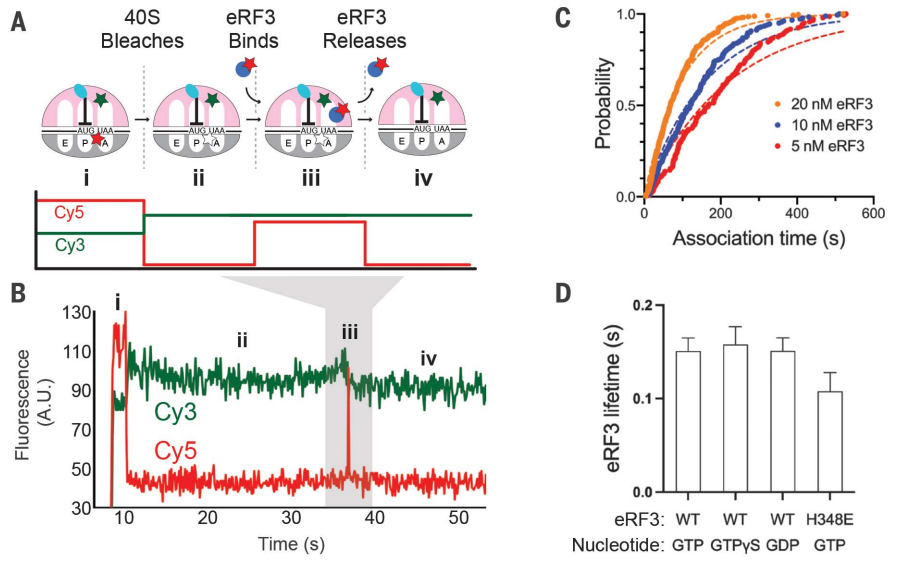

Fig. 3. Observing eRF3 dynamics in ZMWs. (**A**) Assay schematic. (**B**) Example of eRF3 binding to M-Stop ribosomes. (**C**) Binding of eRF3 to M-Stop ribosomes is concentration dependent. Association time distributions were fit to an exponential model. (**D**) GTP hydrolysis by eRF3 is not required for its release from the ribosome in the absence of eRF1.

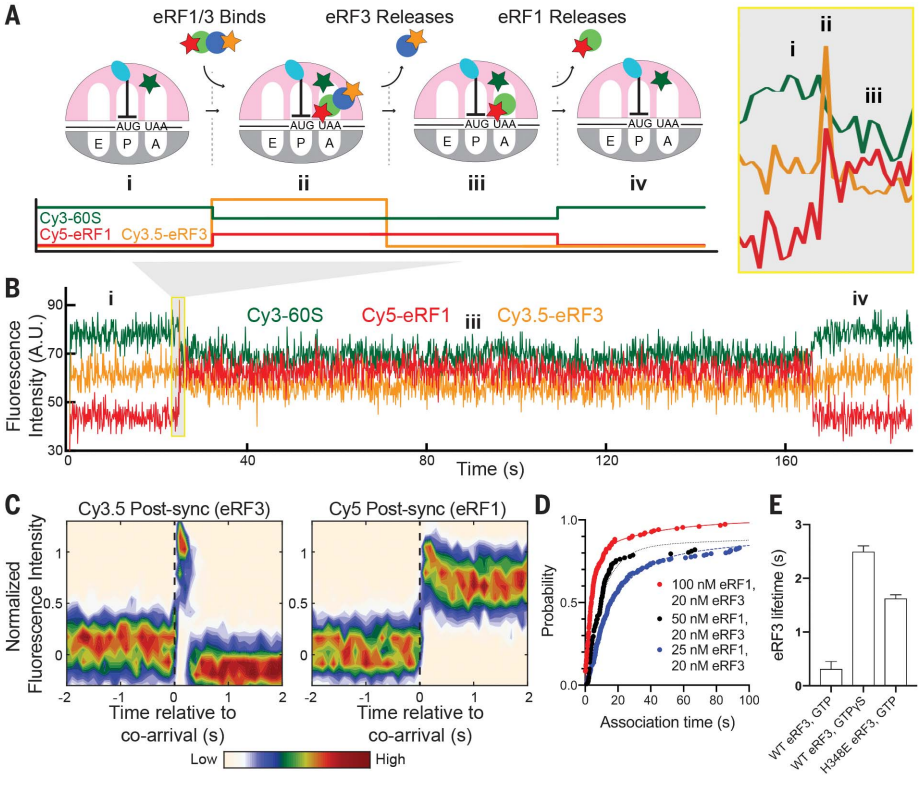

Fig. 4. eRF3 delivers eRF1 quickly to ribosomes halted at stop codons. (**A**) Assay schematic. (**B**) Example of simultaneous binding of eRF1 (Cy5, red) and eRF3 (Cy3.5, yellow) to M-Stop ribosomes (Cy3, green). (**C**) Postsynchronization plot of fluorescence changes observed upon simultaneous binding of eRF1 and eRF3 (dashed, black vertical line). (**D**) Simultaneous binding of eRF1 and eRF3 to M-Stop ribosomes is fast and concentration dependent. Association time distributions were fit to a double-exponential model. (**E**) GTP hydrolysis by eRF3 accelerates its release from the ribosome in the presence of eRF1.

dependence on GTP hydrolysis and ranged from 0.11 to 0.16 s; Fig. 3D), here, GTP accelerated eRF3 release from ribosomes by eightfold compared with experiments performed with the more slowly hydrolyzed analog GTPγS (0.3 ± 0.1 s with GTP versus 2.5 ± 0.1 s with GTPγS; Fig. 4E and fig. S4, E and F). Substitution of wild-type eRF3 with a GTPase-deficient mutant similarly slowed its release from the ribosome by fivefold (1.6 ± 0.1 s; Fig. 4E and fig. S4, E and F). Thus, eRF3 is a chaperone that delivers eRF1 to ribosomes halted at stop codons, and eRF3 departure from the ribosome is partly governed by its GTPase activity.

Real-time monitoring of translation termination

We next sought to understand the timing and regulation of peptidyl-tRNA ester bond hydrolysis catalyzed by eRF1. Peptide hydrolysis triggers rapid rearrangement of P-site tRNA from a classical (P/P) to a hybrid (P/E) state (*18*), and we hypothesized this rearrangement could be tracked using FRET between labeled P-site–bound tRNA and A-site–bound eRF1 (~34 Å separation before versus ~50 Å after rearrangement; Fig. 5A). To test this, we tethered to ZMWs ribosomes programmed on an M-Stop mRNA with Cy3-labeled Met-tRNA$^{Met}_{i}$ (FRET donor) in the P site; added catalytically inactive Cy5-eRF1 (G180A, FRET acceptor), unlabeled eRF3, and GTP; and illuminated with a 532-nm laser. As expected, high FRET was observed between the classical state tRNA and eRF1 (μ = 0.63, σ = 0.10; Fig. 5B). Next, we repeated the assay but added puromycin, a drug that cleaves the peptidyl-tRNA bond, and indeed observed lower-efficiency FRET between the now hybrid-state tRNA and catalytically inactive eRF1 (μ = 0.53, σ = 0.10; Fig. 5B). Therefore, peptidyl-tRNA bond status can be deduced by monitoring P-site tRNA conformation with respect to eRF1 through this FRET signal.

We used this FRET signal to correlate eRF1 dynamics with peptidyl-tRNA bond hydrolysis in real time. Ribosomes programmed on 5′-biotinylated M-F-Stop mRNAs were tethered to ZMWs and illuminated with a 532-nm laser. We then added a mixture of Cy3-labeled Phe-tRNA^{Phe} (FRET donor), Cy5-eRF1 (FRET acceptor), excess eRF3, elongation factors, and eIF5A [an accessory factor that accelerates elongation and termination (*19*)]. Fast tRNA binding, denoted by high Cy3 signal, was observed soon after factor addition and persisted until translocation and subsequent eRF1 binding occurred (Fig. 5, C and D, and fig. S5A). Association of eRF1 initially resulted in a high-FRET signal (μ = 0.67, σ = 0.07; herein referred to as the "pretermination state"; fig. S5, B and C) and was followed by a lower-FRET signal (μ = 0.46, σ = 0.11; "post-termination

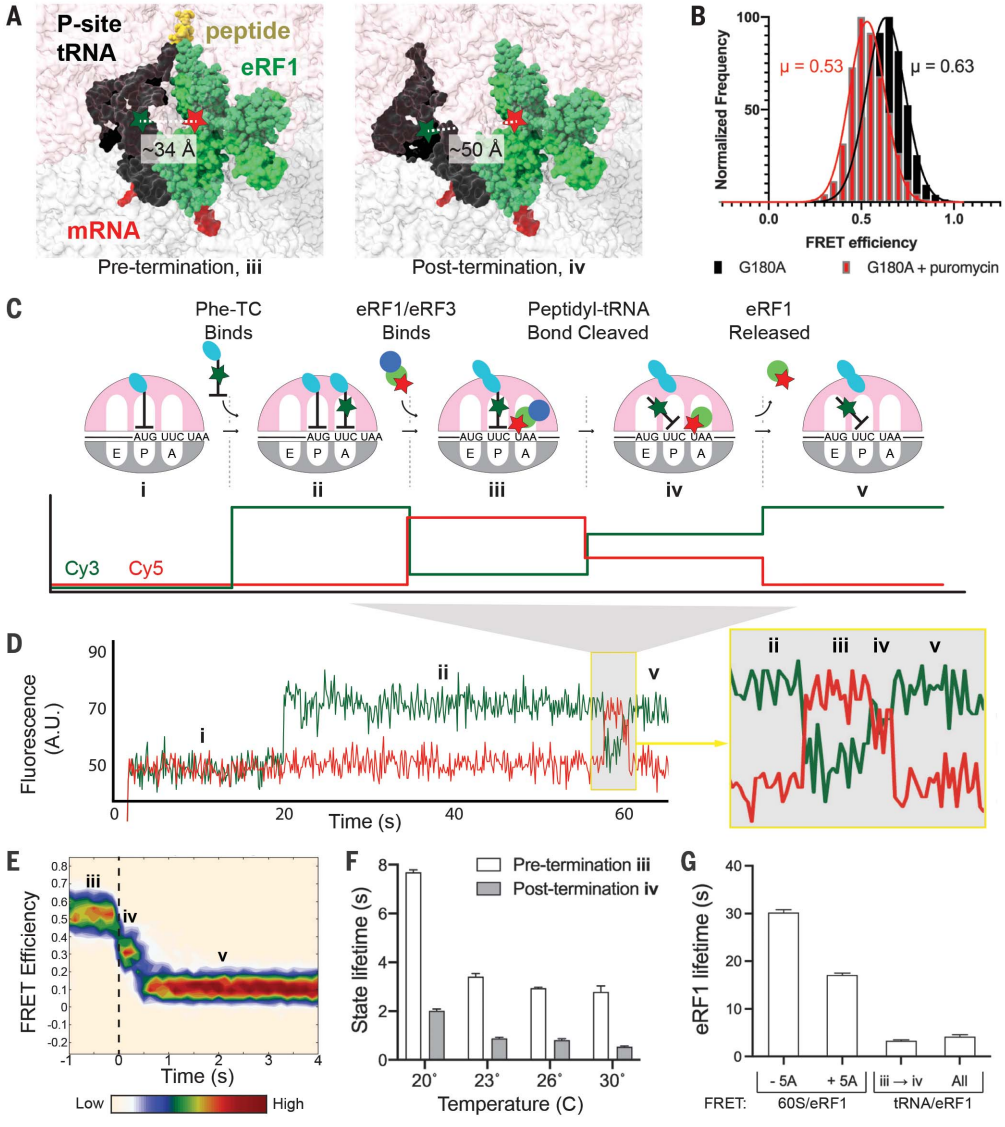

Fig. 5. Tracking peptidyl-tRNA bond hydrolysis. (**A**) Model of FRET between eRF1 (Cy5, red star) and P-site tRNA (Cy3, green star) before and after termination. Left, pretermination [modeled by 40*S* alignment; PDB IDs: 5LZU and 5LZT (*3*, *15*)]. Right, post-termination [modeled by 40*S* alignment; PDB IDs: 5LZU and 3J77 (*15*, *20*)]. (**B**) FRET observed between P-site Cy3-Met-tRNA^{i} and G180A Cy5-eRF1 (black). The addition of puromycin (red) yielded lower FRET, as expected. (**C**) Assay schematic. (**D**) Example of FRET observed with Cy3-Phe (green) and Cy5-eRF1 (red). (**E**) Postsynchronization plot of FRET efficiency observed before and after peptidyl-tRNA bond hydrolysis (dashed, black vertical line). (**F**) Pre- and post-termination state lifetimes observed at different temperatures. (**G**) Dependence of eRF1 lifetime on eIF5A and detection methods. eRF1 lifetimes observed using tRNA/eRF1 FRET either represent all binding events (all) or only those resulting in termination (iii → iv).

state"; Fig. 5, C to E, and fig. S5B). Finally, eRF1 was released from the ribosome, resulting in restoration of high Cy3 signal (Fig. 5, C to E). Critically, substitution of eRF1 with an inactive mutant reduced the number of observed high- to lower-FRET transitions by about sevenfold (fig. S5, D and E), which closely matched the relative extent of peptide release observed in bulk with either wild-type or G180A eRF1 (Fig. 1B and fig. S1, E and F). P-site tRNA/eRF1 FRET is also specific for stop codon recognition, because replacement of the UAA stop codon with near-cognate UAU completely eliminated these FRET transitions (fig. S5D).

We used this tRNA/eRF1 FRET assay to characterize the kinetics of peptidyl-tRNA bond hydrolysis, focusing on ribosomal events before and after termination. Pretermination state lifetimes of eRF1 on the 80*S* ribosome fit well to a two-step, irreversible kinetic model with termination occurring in 2.8 s at 30°C (95% CI: 2.6 to 3.0 s; Fig. 5F and fig. S5, F and G). eRF1 dissociation kinetics, fit to a single-step model by a single exponential, revealed that eRF1 is released quickly after termination in 0.5 s (95% CI: 0.5 to 0.6 s, Fig. 5F and fig. S5, G and H); eRF1 lifetime was unaffected by laser power variation, showing that its lifetime is not limited by dye photobleaching; fig. S5I). Further support that peptidyl-tRNA bond hydrolysis favors eRF1 release was observed with catalytically inactive eRF1, which resided sixfold longer on ribosomes (fig. S5J). Peptidyl-tRNA bond cleavage also hindered rebinding of eRF1 (fig. S5K), demonstrating that termination decreases the affinity of eRF1 for ribosomes. The long eRF1 lifetime observed in our prior measurements (Figs. 2 and 4) is attributable to differences in detection methods and the omission of eIF5A from those assays, because eIF5A does not affect eRF1 association rates but does enhance termination and eRF1 release rates (Fig. 5G and fig. S6) (*19*). Peptidyl-tRNA bond hydrolysis rates increased with temperature from 20 to 30°C (Fig. 5F and figs. S5G and S7, A to C), and subsequent Eyring and Gibbs analyses revealed that termination is regulated by a step with a large energetic barrier (fig. S7D); consistent with this notion, previous structural work demonstrated that eRF1 undergoes a large-scale conformational change (referred to as "accommodation") to render it catalytically active (*3*, *15*), and the tRNA rearrangement tracked by this assay would also depend upon transition of the ribosome from a classical to a hybrid state (*20*). Release of eRF1 from the ribosomal A site is also energetically costly (Fig. 5F and fig. S7E), likely because of extensive interactions that anchor eRF1 to the stop codon (*3*). Termination proceeded at a similar rate when the UAA stop codon was changed to either UAG or UGA (fig. S8), suggesting that a common mechanism is used at all three stop codons. We therefore observed an ordered series of events

at stop codons, with eRF1 eliciting peptidyl-tRNA bond cleavage within ~3 s of ribosomal association, followed by rapid eRF1 release.

Stop codon readthrough effectors slow termination dynamics

We next explored the impact of cis-acting mRNA elements on termination. Prior work uncovered a class of 3′ untranslated region (UTR) mRNA sequences that promote stop codon readthrough (*21*, *22*), but it is unclear whether these elements function in part by inhibiting termination. Indeed, insertion of a six-nucleotide sequence that promotes stop codon readthrough with 30% efficiency (CAAUUA) into the 3′ UTR of M-F-Stop mRNAs lengthened pretermination state duration by twofold (5.9 s, 95% CI: 5.2 to 7.0 s with CAAUUA versus 2.9 s, 95% CI: 2.7 to 3.0 s without CAAUUA; Fig. 6A and fig. S9, A and B). Insertion of other sequences that promote readthrough at lower efficiencies also lengthened the pretermination state, albeit to a lesser degree (Fig. 6A and fig. S9, A and B). Thus, sequences that enhance stop codon readthrough hinder peptidyl-tRNA bond cleavage by eRF1.

The aminoglycosides paromomycin and G418 also promote stop codon readthrough (*23*), primarily by stabilizing near-cognate tRNA in the A site. Paromomycin also inhibits bacterial termination (*24*), but its effects on eukaryotic termination were not deeply characterized (*25*). G418 was recently identified as a eukaryotic termination inhibitor by bulk biochemical studies with a mixed mammalian system (*26*); however, its mode of action remains unclear. We therefore applied our suite of assays to determine the effects of these drugs on eukaryotic termination. The addition of 1 mM G418 [median effective concentration (EC_{50}) of ~2 mM (*27*)] lengthened the pre- and post-termination state duration (each by threefold; Fig. 6B and fig. S9, C to E). Similarly, 50 μM paromomycin [EC_{50} of ~35 μM (*27*)] increased the pretermination state duration (by nearly twofold; Fig. 6C and fig. S9, C to E) and lengthened post-termination state duration (by fivefold; Fig. 6C and fig. S9, C to E). Titration of paromomycin revealed concentration-dependent effects of the drug on post-termination state duration (Fig. 6C and fig. S9, C to E). Simultaneous tracking of eRF1/eRF3 dynamics (as described in Fig. 4) revealed that 50 μM paromomycin slowed eRF1/eRF3 co-binding to the ribosome (by more than twofold; fig. S9F). Together, these studies demonstrate that stop codon readthrough effectors hinder numerous facets of termination, thus uncovering additional nodes to target with potential therapeutics.

Discussion

Whereas prior work broadly described the roles of eRF1 and eRF3 in regulating eukaryotic termination (*2*, *4*, *5*, *19*, *28*), here, we directly monitored the kinetics of individual substeps to obtain a higher-resolution view of this essential process (Fig. 6D). First, a prebound ternary complex of eRF1, eRF3, and GTP rapidly binds to a ribosome halted at a stop codon (Figs. 2 and 4). eRF3 appears to unlock eRF1 conformation to facilitate fast ribosomal binding, because the association of eRF1 alone is slow and governed by an eRF1 concentration–independent event (Fig. 2, D and E). Consistent with this notion, prior structural studies demonstrated that the predominant conformation of eRF1 free in solution is incompatible with ribosomal binding (fig. S10) (*3*, *15*, *29*, *30*). Next, eRF3 hydrolyzes GTP to promote its own release (Fig. 4E), which permits the rearrangement of eRF1 to an active conformation (*15*). Accommodated eRF1 then rapidly cleaves the peptidyl-tRNA bond, triggering ribosomal intersubunit rotation, movement of the deacylated P-site tRNA to a P/E hybrid state, and ejection of both eRF1 and the liberated peptide (Fig. 5). Indeed, eRF1 release was slowed by small molecules that hinder ribosomal rotation (G418 and paromomycin; Fig. 6, B and C) (*27*), which further shows the interdependence of these events. Direct tracking of peptidyl-tRNA bond hydrolysis further uncovered how small molecules and mRNA sequences inhibit discrete steps in termination to promote stop codon readthrough (Fig. 6, A to C). With the critical caveat that termination may also be influenced by unidentified nascent chain dynamics and other trans-acting factors, we propose that the termination mechanisms described here are fundamental to eukaryotic translation, because the release factors are widely conserved from yeast to humans (fig. S11) (*1*, *6*).

To assess the physiological relevance of our in vitro results, we compared them with ribosome-profiling measurements that report A-site occupancy using the ratio of short (21 nucleotides: empty A site) versus long (28 nucleotides: occupied A site) ribosome-protected footprints (RPFs). Prior studies suggested that binding of eRF1 to ribosomes is not rate limiting for termination, because long RPFs substantially outnumber short RPFs at stop codons (*31*). We confirmed this hypothesis through direct observation of termination substeps (Fig. 6D), which demonstrated that release factor binding is indeed faster than subsequent ribosomal events. The finding that termination (~4 s) is fast relative to initiation [~20 to 60 s (*32*, *33*)] but somewhat slower than elongation [0.05 to 1.4 s per codon (*33*)] suggests the existence of an intricate choreography that prevents the accumulation of ribosomes at stop codons. Consistent with this, ribosomal profiling in eRF1-depleted cells revealed a marked increase in queueing of ribosomes at stop codons (*31*).

Eukaryotic termination differs substantially from the mechanisms described previously for bacterial termination, in which the bacterial namesake of eRF3, RF3, drives the departure of eRF1-like factors (RF1/2) from ribosomes (*34*). Instead, eukaryotic termination more closely resembles translation elongation (*5*), in which bacterial EF-Tu and eukaryotic eEF1A assist in the selection of proper tRNAs through a tightly regulated, multistep process. In eukaryotic termination, eRF3 (itself an EF-Tu/eEF1A homolog) in complex with GTP quickly delivers eRF1

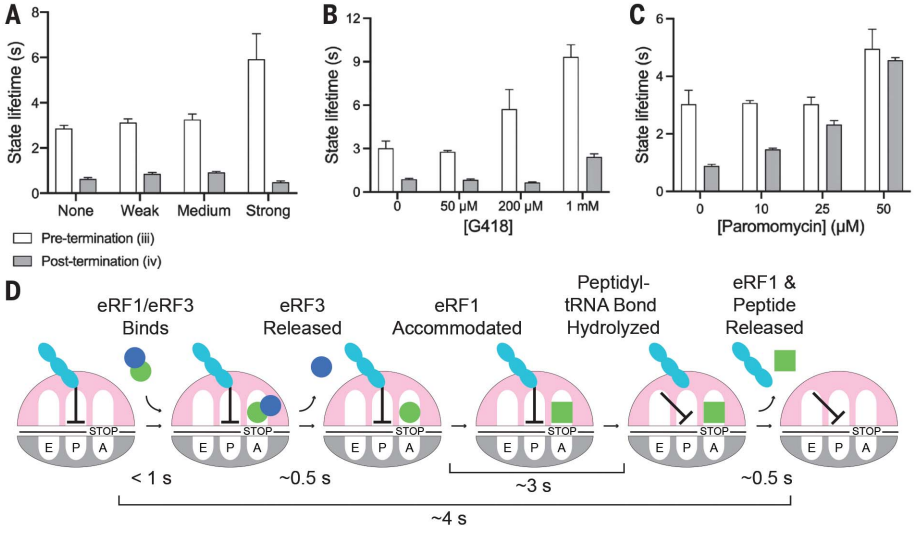

Fig. 6. Termination is regulated by release factors, 3′ UTR mRNA sequence, and small molecules. (**A**) Insertion of 3′ UTR mRNA sequences known to promote stop codon readthrough ("weak," CAAAGA, 10% efficiency; "medium," CAAUCA, 20% efficiency; and "strong," CAAUUA, 30% efficiency) hinder termination; eRF1 release is unaffected. (**B** and **C**) The aminoglycosides G418 (B) and paromomycin (C) slow termination and eRF1 release. (**D**) Order and timing of events in eukaryotic termination.

(a tRNA-shaped protein) to a stop codon in the A site (Fig. 4, A and B), similar to the rapid association of eEF1A/tRNA/GTP ternary complex with a sense codon in the A site. eRF3 hydrolyzes GTP to promote its release from the ribosome and facilitate eRF1 accommodation (Fig. 4E) (*15*), just as EF-Tu and eEF1A hydrolyze GTP to accelerate their ejection and favor tRNA accommodation (*35*, *36*). Thus, the similarities between elongation and eukaryotic termination are not limited to factor architecture, but also include the molecular choreography of these processes.

The fidelity of translation elongation is driven in part by kinetic proofreading, in which EF-Tu/eEF1A preferentially rejects noncognate tRNAs in two sequential steps to boost overall accuracy (*35*–*37*). Although the basis of termination fidelity is unknown, we consider kinetic proofreading a plausible model. eRF3 is essential for termination fidelity, because its inclusion boosts specificity by 2600-fold (*28*). Here, we show that eRF3 conformationally unlocks and delivers eRF1 to ribosomes (Figs. 2 and 4) and facilitates eRF1 accommodation in an eRF3 GTPase–dependent manner (Fig. 4), thus providing eRF3 with multiple opportunities to favor genuine stop codons. Further study of termination substep kinetics at cognate and near-cognate stop codons will reveal whether proofreading governs eukaryotic termination fidelity.

Mutations that introduce a premature stop codon pose a distinct challenge for therapeutic intervention. These mutations trigger premature termination, liberating an incomplete polypeptide, and the defective mRNAs are further degraded by nonsense-mediated decay (NMD) (*38*). To achieve effective therapeutic readthrough of premature stop codons, elongation, termination, and NMD must all be carefully tuned to avoid widespread misregulation of gene expression while still eliciting enough readthrough to alleviate disease. Thus, termination and NMD inhibitors may prove most useful as adjuvants, lengthening the kinetic window for drug-mediated readthrough of premature stop codons. Extension of these single-molecule assays to monitor stop codon readthrough and NMD will provide the quantitative tools necessary to evaluate combination therapies, paving the way to effective treatments.

REFERENCES AND NOTES

1. L. Frolova *et al*., *Nature* **372**, 701–703 (1994).
2. E. Z. Alkalaeva, A. V. Pisarev, L. Y. Frolova, L. L. Kisselev, T. V. Pestova, *Cell* **125**, 1125–1136 (2006).
3. A. Brown, S. Shao, J. Murray, R. S. Hegde, V. Ramakrishnan, *Nature* **524**, 493–496 (2015).
4. C. J. Shoemaker, R. Green, *Proc. Natl. Acad. Sci. U.S.A.* **108**, E1392–E1398 (2011).
5. D. E. Eyler, K. A. Wehner, R. Green, *J. Biol. Chem.* **288**, 29530–29538 (2013).
6. G. Zhouravleva *et al*., *EMBO J.* **14**, 4065–4072 (1995).
7. A. Heuer *et al*., *Nat. Struct. Mol. Biol.* **24**, 453–460 (2017).
8. T. Becker *et al*., *Nature* **482**, 501–506 (2012).
9. K. M. Keeling, X. Xue, G. Gunn, D. M. Bedwell, *Annu. Rev. Genomics Hum. Genet.* **15**, 371–394 (2014).
10. M. Mort, D. Ivanov, D. N. Cooper, N. A. Chuzhanova, *Hum. Mutat.* **29**, 1037–1047 (2008).
11. R. Bordeira-Carriço, A. P. Pêgo, M. Santos, C. Oliveira, *Trends Mol. Med.* **18**, 667–678 (2012).
12. M. G. Acker, S. E. Kolitz, S. F. Mitchell, J. S. Nanda, J. R. Lorsch, *Methods Enzymol.* **430**, 111–145 (2007).
13. Methods and materials are available as supplementary online materials.
14. J. Wang *et al*., *Nature* **573**, 605–608 (2019).
15. S. Shao *et al*., *Cell* **167**, 1229–1240.e15 (2016).
16. S. Uemura *et al*., *Nature* **464**, 1012–1017 (2010).
17. J. Chen *et al*., *Proc. Natl. Acad. Sci. U.S.A.* **111**, 664–669 (2014).
18. J. Flis *et al*., *Cell Rep.* **25**, 2676–2688.e7 (2018).
19. A. P. Schuller, C. C. Wu, T. E. Dever, A. R. Buskirk, R. Green, *Mol. Cell* **66**, 194–205.e5 (2017).
20. E. Svidritskiy, A. F. Brilot, C. S. Koh, N. Grigorieff, A. A. Korostelev, *Structure* **22**, 1210–1218 (2014).
21. O. Namy, I. Hatin, J. P. Rousset, *EMBO Rep.* **2**, 787–793 (2001).
22. O. Namy *et al*., *Nucleic Acids Res.* **31**, 2289–2296 (2003).
23. J. R. Wangen, R. Green, *eLife* **9**, e52611 (2020).
24. E. M. Youngman, L. Cochella, J. L. Brunelle, S. He, R. Green, *Cold Spring Harb. Symp. Quant. Biol.* **71**, 545–549 (2006).
25. D. E. Eyler, R. Green, *RNA* **17**, 925–932 (2011).
26. D. Susorov, S. Egri, A. A. Korostelev, *RNA* **26**, 2044–2050 (2020).
27. I. Prokhorova *et al*., *Proc. Natl. Acad. Sci. U.S.A.* **114**, E10899–E10908 (2017).
28. G. Indrisiunaite, Dissertation, Faculty of Science and Technology, Uppsala University (2019).
29. H. Song *et al*., *Cell* **100**, 311–321 (2000).
30. Z. Cheng *et al*., *Genes Dev.* **23**, 1106–1118 (2009).
31. C. C. Wu, B. Zinshteyn, K. A. Wehner, R. Green, *Mol. Cell* **73**, 959–970.e5 (2019).
32. P. Shah, Y. Ding, M. Niemczyk, G. Kudla, J. B. Plotkin, *Cell* **153**, 1589–1601 (2013).
33. D. Chu *et al*., *EMBO J.* **33**, 21–34 (2014).
34. D. V. Freistroffer, M. Y. Pavlov, J. MacDougall, R. H. Buckingham, M. Ehrenberg, *EMBO J.* **16**, 4126–4133 (1997).
35. T. Pape, W. Wintermeyer, M. V. Rodnina, *EMBO J.* **17**, 7490–7497 (1998).
36. T. Pape, W. Wintermeyer, M. Rodnina, *EMBO J.* **18**, 3800–3807 (1999).
37. A. B. Loveland, G. Demo, A. A. Korostelev, *Nature* **584**, 640–645 (2020).
38. F. He, A. Jacobson, *Mol. Cell. Biol.* **21**, 1515–1530 (2001).
39. J. Yin *et al*., *Proc. Natl. Acad. Sci. U.S.A.* **102**, 15815–15820 (2005).
40. E. Gutierrez *et al*., *Mol. Cell* **51**, 35–45 (2013).
41. C. J. Shoemaker, D. E. Eyler, R. Green, *Science* **330**, 369–372 (2010).
42. P. Tesina *et al*., *EMBO J.* **39**, e103365 (2020).
43. J. Wang *et al*., *Nat. Commun.* **11**, 5003 (2020).
44. V. A. Mitkevich *et al*., *Nucleic Acids Res.* **34**, 3947–3954 (2006).
45. A. V. Kononenko *et al*., *Nucleic Acids Res.* **38**, 548–558 (2010).
46. B. Ho, A. Baryshnikova, G. W. Brown, *Cell Syst.* **6**, 192–205.e3 (2018).
47. P. Jorgensen, J. L. Nishikawa, B. J. Breitkreutz, M. Tyers, *Science* **297**, 395–400 (2002).
48. A. G. Johnson *et al*., *RNA* **25**, 881–895 (2019).
49. O. V. Korobov, *Chemical Kinetics with Mathcad and Maple* (Springer, 2011).
50. A. Petrov, R. Grosely, J. Chen, S. E. O'Leary, J. D. Puglisi, *Mol. Cell* **62**, 92–103 (2016).
51. R. A. Marshall, M. Dorywalska, J. D. Puglisi, *Proc. Natl. Acad. Sci. U.S.A.* **105**, 15364–15369 (2008).
52. C. E. Aitken, J. D. Puglisi, *Nat. Struct. Mol. Biol.* **17**, 793–800 (2010).
53. M. F. Juette *et al*., *Nat. Methods* **13**, 341–344 (2016).
54. J. E. Bronson, J. Fei, J. M. Hofman, R. L. Gonzalez Jr., C. H. Wiggins, *Biophys. J.* **97**, 3196–3205 (2009).
55. J. Choi, J. D. Puglisi, *Proc. Natl. Acad. Sci. U.S.A.* **114**, 13691–13696 (2017).
56. H. S. Steinert, J. Rinnenthal, H. Schwalbe, *Biophys. J.* **102**, 2564–2574 (2012).
57. J. Rinnenthal, B. Klinkert, F. Narberhaus, H. Schwalbe, *Nucleic Acids Res.* **38**, 3834–3847 (2010).
58. C. Magis *et al*., *Methods Mol. Biol.* **1079**, 117–129 (2014).
59. E. F. Pettersen *et al*., *Protein Sci.* **30**, 70–82 (2021).
60. P. Saini, D. E. Eyler, R. Green, T. E. Dever, *Nature* **459**, 118–121 (2009).
61. M. H. Park, H. L. Cooper, J. E. Folk, *Proc. Natl. Acad. Sci. U.S.A.* **78**, 2869–2873 (1981).

ACKNOWLEDGMENTS

We thank C. Lapointe, C. Preston, and A. Gilliam Valentic for editing assistance and members of the Puglisi and Green laboratories for discussions and input. **Funding:** This work was supported by the A.P. Giannini Foundation (postdoctoral fellowship to M.R.L.), the Cystic Fibrosis Foundation (grant PUGLISI20GO to J.D.P.), and the National Institute of General Medical Sciences (grant R37GM059425 to R.G. and grants R01GM113078 and R01GM51266 to J.D.P.). **Author contributions:** M.R.L., L.N.L., R.G., and J.D.P. conceived the project. M.R.L., L.N.L., and J.W. generated reagents with guidance from R.G. and J.D.P. L.N.L. performed and analyzed bulk peptide release experiments with guidance from R.G. M.R.L. performed and analyzed all single-molecule experiments (except those for fig. S2G, which were done by J.W.) with guidance from J.W., A.P., and J.D.P. N.C.C. contributed custom single-molecule data analysis scripts. M.R.L. and L.N.L. prepared the figures and drafted the initial manuscript, which was revised with input from J.W., A.P., R.G., and J.D.P. All authors read and approved the final manuscript. **Competing interests:** The authors declare no competing interests. **Data and materials availability:** All data are available in the main text or the supplementary materials. Relevant expression constructs are available upon request.

SUPPLEMENTARY MATERIALS

science.sciencemag.org/content/373/6557/876/suppl/DC1
Materials and Methods
Figs S1 to S11
Table S1
References (*39*–*61*)
MDAR Reproducibility Checklist

View/request a protocol for this paper from *Bio-protocol*.

2 April 2021; accepted 7 July 2021
10.1126/science.abi7801

Mechanisms that ensure speed and fidelity in eukaryotic translation termination

Michael R. LawsonLaura N. LessenJinfan WangArjun PrabhakarNicholas C. CorsepiusRachel GreenJoseph D. Puglisi

Science, 373 (6557), • DOI: 10.1126/science.abi7801

How translation stops

Protein synthesis concludes when a ribosome encounters a stop codon in a transcript, which triggers the recruitment of highly conserved release factors to liberate the protein product. Lawson *et al*. used traditional biochemical methods and single-molecule fluorescence assays to track the interplay of release factors with ribosomes and reveal the molecular choreography of termination. They identified two distinct classes of effectors, small molecules and mRNA sequences, that directly inhibited the release factors and promoted stop codon readthrough. These findings may buttress ongoing efforts to treat diseases caused by premature stop codons, which cause 11% of all heritable human diseases. —DJ

Science (ISSN) is published by the American Association for the Advancement of Science. 1200 New York Avenue NW, Washington, DC 20005. The title *Science* is a registered trademark of AAAS.